THE JOURNAL OF PHYSICAL CHEMISTRY A

Article

Competition between HO2 and H2O2 Reactions with CH2OO/anti-CH3CHOO in the Oligomer Formation: A Theoretical Perspective

Long Chen, Yu Huang, Yonggang Xue, Jun-ji Cao, and Wenliang Wang

J. Phys. Chem. A, **Just Accepted Manuscript** • DOI: 10.1021/acs.jpca.7b05951 • Publication Date (Web): 24 Aug 2017

ACS Publications

The Journal of Physical Chemistry A is published by the American Chemical Society. 1155 Sixteenth Street N.W., Washington, DC 20036

Competition between HO_2 and H_2O_2 Reactions with CH_2OO/*anti*-CH_3CHOO in the Oligomer Formation: A Theoretical Perspective

Long Chen [a, b], Yu Huang [a, b, *], Yonggang Xue [a, b], Junji Cao [a,b, *], Wenliang Wang [c]

[a] *Key Lab of Aerosol Chemistry & Physics, Institute of Earth Environment, Chinese Academy of Sciences, Xi'an, Shaanxi, 710061, China*

[b] *State Key Laboratory of Loess and Quaternary Geology, Institute of Earth Environment, Chinese Academy of Sciences, Xi'an 710061, China*

[c] *School of Chemistry and Chemical Engineering, Key Laboratory for Macromolecular Science of Shaanxi Province, Shaanxi Normal University, Xi'an, Shaanxi, 710119, China*

*Corresponding author:

Prof. Yu Huang, E-mail address: huangyu@ieecas.cn

Prof. Junji Cao, E-mail address: cao@loess.llqg.ac.cn

Tel: + 86-29-62336261, Fax: + 86-29-62336261.

Abstract:

Understanding Criegee chemistry has become one of the central topics in atmospheric studies recently. Ozonolysis of unsaturated hydrocarbons is believed to be an important pathway of SOA. However, the SOA formation mechanisms *via* Criegee chemistry are still poorly understood. Here, we systematically study the competition between HO_2 and H_2O_2 reactions with CH_2OO/*anti*-CH_3CHOO in the oligomer formations. The calculated results show that oligomers having Criegee intermediates as the chain units are produced by the sequential addition of CIs to HO_2 and H_2O_2 molecules. The addition reactions are predicted to be strongly exothermic and the apparent activation barriers are estimated to be much negative, suggesting that these reactions are feasible both thermochemically and dynamically. Compared to the barriers of $4CH_2OO + HO_2$ and $4CH_2OO + H_2O_2$ reactions, it can be found that the first two CH_2OO addition reactions in the former case are favoured, while the last two CH_2OO addition reactions in the latter case are preferable. Similar conclusion is also obtained from those of the 4*anti*-$CH_3CHOO + HO_2/H_2O_2$ systems. The mechanistic insights can motivate future experimental studies of the effect of longer chains CIs on the formation of SOA which plays an important role on air quality and climate change.

1. Introduction

Secondary organic aerosol (SOA) contributed 33-77% of the mass concentration of $PM_{2.5}$ during haze episodes experienced over China megacities[1-3], which is formed by photochemical oxidation of unsaturated volatile organic compounds (VOCs). Criegee intermediates (CIs), also called as carbonyl oxides, are generated by ozonolysis of unsaturated hydrocarbons[4-7]. The formed CIs are characterized by high intrinsic reactivity and excess vibrational energies[8], which can easily react with a number of atmospheric species such as SO_2[9-10], H_2O[11-12], RO_x[13] and so forth. These bimolecular reactions are believed to play crucial role in the tropospheric budgets of organic acids[14], hydroxyl radicals[15], sulfates, and SOA[16]. The hydroperoxy radical (HO_2) is a prototypical example of the peroxy radical (RO_2) because it is the most abundant RO_2 radical in the atmosphere and plays an important role in ozone cycle and hydrogen peroxide (ROOH) formation[17]. The atmospheric concentration of HO_2 radical is predicted to be 10^6-10^8 molecules cm^3,[18] which is generated through the excited oxygen atoms reaction with water vapor and the red light induced decomposition of α-hydroxy methylperoxy radical ($OHCH_2(O)_2$)[17-19]. The bimolecular reaction of CI with HO_2 radical is one of the dominant sinks of carbonyl oxide and plays a significant impact on the formation of oligomers, which have sufficiently low volatility and highly oxygenated to potentially affect SOA formation and growth[1,6,13]. In addition to these gas phase reactions, there is a large body of experimental and theoretical literatures on the Criegee chemistry at the air/water interface, air/aqueous interface and aqueous organic surface. For example, CH_2OO + H_2O[20], CH_2OO + H_2S[21], syn-/anti-CH_3CHOO + H_2O[22], CIs + cis-Pinonic acid (CPA)[23] reactions etc. These reactions follow both loop-structure-mediated and stepwise mechanisms with former being the dominant mechanistic pathway.

Recently, experimental studies have proposed that oligomers containing SCI as the chain units are the dominant components of SOA[24-25]. However, the formation mechanisms of oligomer $ROO(CH_2OO)_nH$ are not consistent. Sadezky et al.[24] proposed that the mechanism contains sequential addition of CH_2OO to RO_2 radical

leading to the $ROO(CH_2OO)_n$ radical adduct, then the oligomer $ROO(CH_2OO)_nH$ is formed by abstraction a hydrogen atom from HO_2 radical to complete chain termination.

$$RO_2 + CH_2OO \rightarrow ROO\text{-}CH_2OO \quad (1)$$

$$ROO\text{-}CH_2OO + (n\text{-}1)CH_2OO \rightarrow ROO\,(CH_2OO)_{n-1}CH_2OO \quad (2)$$

$$ROO\,(CH_2OO)_{n-1}CH_2OO + HO_2 \rightarrow ROO\,(CH_2OO)_nH + O_2 \quad (3)$$

However, Sakamoto et al.[25] proposed a new oligomer formation mechanism involving sequential addition of CH_2OO to ROOH molecule instead of to RO_2 radical. Wolff et al.[26] concluded the same by the gas phase ozonolysis of ethene that the reaction of CH_2OO with HOOH leading to the formation of hydroperoxy-methyl hydroperoxides.

$$ROOH + CH_2OO \rightarrow ROO\text{-}CH_2OO\text{-}H \quad (4)$$

$$ROO\text{-}CH_2OO\text{-}H + (n\text{-}1)\,CH_2OO \rightarrow ROO(CH_2OO)_nH \quad (5)$$

It is essential to investigate the reaction pathways regarding to the formation and growth of oligomer, which is highly oxygenated and can influence SOA formation eventually.

To the best of our knowledge, the sequential addition of small Criegee intermediates (CH_2OO and *anti*-CH_3CHOO) to HO_2 and H_2O_2 molecules leading to the formations of oligomers have not been reported using theoretical methodologies. In addition, there are no studies discussing the competition between HO_2 and H_2O_2 reactions with CH_2OO/*anti*-CH_3CHOO under atmospheric conditions. Recently, a theoretical study on the reaction mechanism between CH_2OO and HO_2 radical has been investigated at the CCSD(T)/6-311++G(3df,2p)//B3LYP/6-311++G(d,p) level of theory by Long and co-workers[13]. The calculated results indicated that the favorable route in the bimolecular reaction of CH_2OO with HO_2 is proton transfer plus the addition reaction channel with a barrier of 1.6 kcal·mol^{-1}. Vereecken et al.[6] and Anglada et al.[27] investigated the bimolecular reaction of CH_3OO with CH_2OO by means of different quantum chemical methods. The calculated results showed that the

barrier for the addition of CH_3OO terminal oxygen atom to the CH_2OO carbon atom leading to the CH_3OOCH_2OO radical adduct is comparatively low (< 1.5 kcal·mol^{-1}). All these works provide important references to deeper understand the oligomer formation mechanism. Unfortunately, in Long's study[13], the addition reaction between CH_2OO and HO_2 is merely considered in the presence of single CH_2OO intermediate, while the effect of two or more CH_2OO intermediates on the oligomer formation were not taken into consideration. Moreover, a quantitative evaluation of the atmospheric importance of the CH_2OO/*anti*-CH_3CHOO + HO_2/H_2O_2 reactions is not possible at the moment because the experimental and theoretical rate coefficients are not available.

The main goal of this work is to explore the mechanism of oligomer formation for Criegee chemistry in the gas phase, which is investigated in light of theoretical predictions. We mainly consider the competition reaction pathways between HO_2/H_2O_2 and CH_2OO/*anti*-CH_3CHOO, in which CI serve as the repeat unit (n=4) in the formation of oligomer. We choose the simplest HO_2 radical as a proxy for small RO_2 radicals because it is one of the biggest oxidants and plays an important role in the radical-radical reaction in the atmosphere[13].

2. Computational methods

The quantum chemical calculations are executed using the Gaussian 09 electronic structure program[28]. Lee et al.[29] investigated the transient infrared absorption spectrum of the simplest Criegee intermediate CH_2OO, and observed that the vibrational frequencies are more consistent with a zwitterion rather than a diradical structure of CH_2OO. Miliordos et al.[30] and Long et al.[31] concluded the same by the theoretical calculations that CH_2OO is best described as a closed-shell singlet ground electronic state. Thus, in the present work, the B3LYP functional in combination with the 6-311+G(2df,2p) basis set[32] is employed to optimize and characterize the geometries of reactants, intermediates, transition states, and products. The Grimme's dispersion correction method is employed to describe medium range correlation effects[33]. We choose the B3LYP functional because it gives reliable results

for describing the geometries, zero-point energies (ZPE), and frequencies for Criegee chemistry[5,7,34-35]. Harmonic vibrational frequencies are performed to quantify the local minima and transition state that there are zero (NIMAG = 0) and one (NIMAG = 1) imaginary frequencies. A scale factor[35] of 0.986 is applied to scale all the B3LYP-D3/6-311+G(2df,2p) frequencies to account for the thermodynamic contribution to the Gibbs free energy and enthalpy at 298.15 K and 1 atm. The connectivity between the two energy minimum points is established by intrinsic reaction coordinate (IRC) calculations[36-39]. Then, the single point energies are calculated at the MP2 level of theory[40] based on the B3LYP-D3 optimized geometries to further improve the energetics. Finally, the high-pressure limiting (HPL) rate coefficients of conventional transition state theory (TST) with an one-dimensional unsymmetrical Eckart tunneling correction factor[41-43] are calculated by implementing VKLab program[44].

As shown in Fig. 2(a), the bimolecular reaction of CH_2OO with HO_2 mainly includes the following two steps: (i) the formation of intermediate IM1-1 through a barrierless process; (ii) then, it dissociates to the product P1-1 *via* transition state TS1-1. The whole reaction process can be described as eqn (6)[45].

$$CH_2OO + HO_2 \underset{k_{-1}}{\overset{k_1}{\rightleftharpoons}} \text{IM1-1} \xrightarrow{k_2} \text{TS1-1} \rightarrow \text{P1-1} \quad (6)$$

Assuming thermal equilibrium between the reactants (CH_2OO + HO_2) and the VDW complex (IM1-1) is established. The overall rate coefficient can therefore be extrapolated to the eqn (7) using steady state approximation (SSA)[46]:

$$k_{ovr} = \frac{k_1 \times k_2}{k_{-1} + k_2} \quad (7)$$

If $k_2 << k_{-1}$, the overall rate coefficient is written in the eqn (8) as a product of the equilibrium coefficient (K_{eq}) between the reactant and complex, and the rate coefficient (k_2) of the complex IM1-1 decomposing into the product P1-1 using transition state theory (TST)[47-48].

$$k_{ovr} = \frac{k_1 \times k_2}{k_{-1} + k_2} \approx \frac{k_1}{k_{-1}} k_2 = K_{eq} k_2 \quad (8)$$

The equilibrium coefficient K_{eq} can be written as eqn (9):

$$K_{eq} = \sigma \frac{Q_{IM}(T)}{Q_A(T)Q_B(T)} \exp\left(\frac{E_R - E_{IM}}{RT}\right) \quad (9)$$

where σ is reaction symmetry number; $Q_{IM}(T)$, $Q_A(T)$ and $Q_B(T)$ are the partition function for the intermediate, reactants A and B, respectively; T is the temperature in Kelvin; E_R and E_{IM} are the total energies of the reactant and intermediate complex, respectively[46]. Finally, the total rate coefficients are fitted to the modified three parameters Arrhenius expression:

$$k_{tot} = A \times T^n \times \exp(-E_a / RT) \quad (10)$$

3. Results and discussion

The global flux diagram for the oligomer formations in the reactions of CH_2OO/*anti*-CH_3CHOO with HO_2 and H_2O_2 is drawn in Scheme 1. In the potential energy surfaces (PESs), the transition state and intermediate are designated by the prefix TS and IM, respectively. The singlet and triplet species are signed 1 and 3 as superscription. The optimized geometries of some selected stationary points are displayed in Fig. 1 with previous available experimental and theoretical values for comparison. All the geometries are given in Fig. S1-S4. For the species (CH_2OO, H_2O_2, HO_2 and $^3O_2$), the mean absolute deviations (MAD) of bond lengths and angles between the calculated values at the B3LYP-D3/6-311+G(2df,2p) level and the corresponding experimental ones are 0.008 Å and 1.2°, respectively. The largest deviation is 0.018 Å for C=O bond and 1.6° for ∠H-O-O angle in CH_2OO intermediate. These two comparisons show that the B3LYP-D3 functional employed here is sufficient to describe the geometrical parameters. Additionally, the rotational constants of CH_2OO are also listed in Table S1, which agree reasonably well with the experimental and theoretical reports[31]. The result confirms again the above mentioned conclusion that the B3LYP-D3 functional applied is reliable to characterize the mechanisms. Table 1 lists the activation energies ($\Delta E_a^{\#}$), free energies ($\Delta G_a^{\#}$), and reaction enthalpies ($\Delta_r H_m$) of individual elementary reaction involved in the title reaction system. The relative energies plus ZPE (ΔE_R), enthalpies (ΔH_R), and free

energies (ΔG_R) are presented in Table S2-S5. The PESs of HO_2 and H_2O_2 reactions with CH_2OO/*anti*-CH_3CHOO are constructed in Figs. 2 and 4 using the MP2//B3LYP-D3/6-311+G(2df,2p) electronic energies. Experimentally, the singlet O_2 ($^1\Delta_g$) lies 22.6 kcal·mol^{-1} above the ground electronic state $^3\sum_g^-$ [49], whereas it is calculated to be 30.35 kcal·mol^{-1} using the above mentioned method, which is significantly higher than experimental value. Therefore, the energy of O_2 ($^1\Delta_g$) in this work is corrected by summing the relative energy of O_2 ($^3\sum_g^-$) and 22.6 kcal·mol^{-1}. Similar methodology has been adopted by Zhang and co-workers to study the self-reaction of $C_2H_5O_2$ radicals[46].

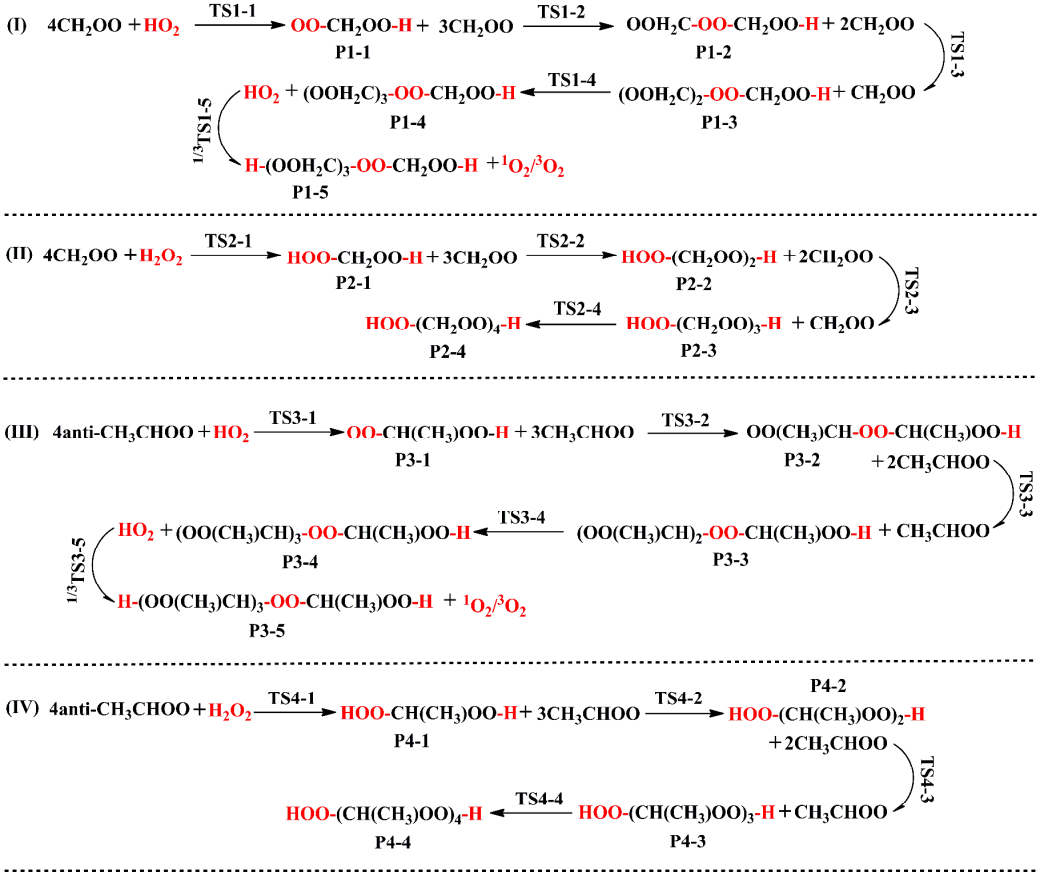

Scheme 1 Brief description for the reactions of CH_2OO/*anti*-CH_3CHOO with HO_2 and H_2O_2

3.1 PES of CH_2OO reactions with HO_2 and H_2O_2

The hydroperoxy radical (HO_2) is one of the most abundant peroxy radicals (RO_2) in the atmosphere and produces through the excited oxygen atoms reaction with water vapor[17]. The simplest alkyl peroxy radical is methyl peroxy radical (CH_3O_2), which is

the most important oxidant in the atmosphere and generates via the oxidation of methane by OH in the presence of O_2[56]. Compared to the CH_3O_2 radical, the HO_2 radical is capable of promoting the hydrogen atom transfer (HAT) reactions because of the hydroxy and peroxy functionalities that allow it to form sterically stable hydrogen bonds with oxygenates[57]. Moreover, the CH_2OO + HO_2 reaction is one of the dominant sinks of carbonyl oxide in some areas and affects the formation of aerosol in the troposphere[13]. Thus, in the present study, we choose the HO_2 radical as a proxy to investigate the detailed mechanism of oligomer formation. The relative energy diagram for the addition reactions of CH_2OO with HO_2 and H_2O_2 is given in Fig. 2 using the MP2//B3LYP/6-311+G(2df,2p) energies.

As seen from Fig. 2, the formations of oligomers P1-5 and P2-4 by which CH_2OO serves as the repeat unit are strongly exothermic (> 220 kcal·mol^{-1}). Moreover, the apparent activation barriers E_{app} of all transition states are negative, signifying that they are energetically feasible under atmospheric condition. This is because the stabilizing interaction remains mostly intact in the addition reaction transition states[6]. Although the oligomers P1-5 and P2-4 are formed by distinct channels, the chemical composition is completely the same. From Fig. 2(a), one can see that the addition reactions of 4CH_2OO + HO_2 begins with the formation of a strong pre-reactive complex IM1-1, of -13.4 kcal·mol^{-1} stability. The IM1-1 is formed by the hydrogen bond interactions between the terminal CH_2OO oxygen atom and the hydrogen of nearby HO_2 ($D_{(O-H)}$=1.622 Å), and between one of the hydrogen atoms in the CH_2OO and the terminal oxygen atom in the HO_2 ($D_{(H-O)}$=2.050 Å) (see Fig. 1). Then, the complex IM1-1 immediately converts into the product P1-1 (OO-CH_2OO-H) via transition state TS1-1 with a barrier of 1.1 kcal·mol^{-1}, which is consistent with the value of 1.0 kcal·mol^{-1} obtained by Long et al.[13] which was obtained at the CCSD(T)/6-311++G(3df,2p)//B3LYP/6-311++G(d,p) level of theory plus BSSE correction. The detailed reaction mechanism includes that the O-O fragment of HO_2 radical moves greatly to approach the CH_2OO carbon atom, whereas the remnant hydrogen atom gets concertedly attached to the terminal oxygen atom, leading to the formation of P1-1 radical adduct (see Scheme 1) and opening the possibility for the

formation of oligomer P1-5. The mechanistic details of the $CH_2OO + HO_2$ reaction are quite similar to that of the gas-phase reactions between CH_2OO and H_2S/H_2O that the addition of H_2S/H_2O across the -COO moiety of CH_2OO occurs in a concerted manner forming $HSCH_2OOH/HOCH_2OOH$ adducts[20-21]. In addition to the well-known concerted one, the $CH_2OO + H_2O/H_2S$ reactions at the air/water interface have been found to follow the stepwise mechanism recently. A comparison of the singly occupied molecular orbitals (SOMOs) of the pre-reactive complex IM1-1 and transition state TS1-1 is presented in Fig. 3. As shown in Fig. 3, the IM1-1 and TS1-1 structures that the electronic activity of HO_2 radical is localized on the lone pair of the oxygen atoms and the CH_2OO is not involved in the SOMO. The orbitals appear to align in a manner consistent with a hydrogen atom transfer (HAT) mechanism. Shenghur et al.[58] concluded the same by investigating the hydrogen abstraction reaction between phenol and nitrogen dioxide. In addition, the evolution of atomic charges as functions of the IRC is studied using natural population analysis (NPA)[59], and the result is presented in Fig. S5. The result shows that the NPA atomic charge on the H-transferred is almost a constant. This conclusion is further supported by previous literature report by Sirjoosingh et al. for HAT reaction[60].

The secondary addition channels R1-2, R1-3, and R1-4 also have similar reaction pathways. The pre-reactive complexes (IM1-2, 1-3, and 1-4) are formed in the entrance channels, and followed by sequential addition of the terminal P1-1 oxygen atom to the CH_2OO carbon atom leading to the products P1-2, P1-3, and P1-4 (see Scheme 1). One can notice that the reaction mechanisms are slightly different from those of the initial reaction R1-1. The barrier heights predict TS1-1, 1-2, 1-3 and 1-4 to lie -12.3, -61.9, -101.8 and -158.9 kcal·mol^{-1}, respectively, below the energies of the separate reactants CH_2OO and HO_2 radical, and 1.1, 2.9, 11.4 and 11.2 kcal·mol^{-1} above the energies of the corresponding pre-reactive complexes IM1-1, 1-2, 1-3 and 1-4. The result shows that the energetically most favourable channel is the first CH_2OO addition reaction R1-1. Similar conclusion is also drawn in the calculated results of Gibbs free energies (see Table 1 and Table S2). Lastly, the P1-4 radical adduct has the unpaired electron localized on the terminal oxygen atom, so it can

abstract the hydrogen atom of HO_2 radical yielding oligomer P1-5 ($HOO\text{-}(CH_2OO)_4\text{-}H$). This reaction proceeds on both the singlet and triplet PESs, with the barriers lying 0.3 and 1.5 kcal·mol^{-1} above the respective complexes ^{1}IM1-5 and ^{3}IM1-5. The result reveals that the oligomer P1-5 formation on the singlet PES is relatively advantaged compared to the triplet PES. As conclusion, the rate-limiting steps are R1-3 and R1-4 of the whole $4CH_2OO + HO_2$ reactions.

Equivalent to the $4CH_2OO + HO_2$ reaction, the polymerization between $4CH_2OO$ and H_2O_2 proceeds by consecutive addition reactions leading to the oligomer P2-4 or P1-5 (see Fig. 2(b)). The addition mechanism involves that the -OOH fragment of H_2O_2 molecule binds to the CH_2OO carbon atom, whereas the remnant hydrogen atom gets concertedly attached to the terminal oxygen atom leading to product P2-1 ($HOO\text{-}CH_2OO\text{-}H$), which, in turn, sequentially reacts with CH_2OO to the final product P2-4. In the sequential addition reactions, the transition state TS2-4 is not located using B3LYP-D3 functional, but it is located at the B3PW91-D3 level of theory and is carefully confirmed using IRC calculations. The HOMO and HOMO-1 of the IM2-1 and TS2-1 is presented in Fig. S6. As shown in Fig. S6, The IM2-1 and TS2-1 structures that the CH_2OO and H_2O_2 are extensively participating in the HOMO and HOMO-1 and the processes are associated with slight charge redistribution. It is interesting to compare the NPA atomic charges in the $CH_2OO + HO_2$ reaction (R1-1) with that for the analogous $CH_2OO + H_2O_2$ reaction (R2-1). It can be found that the changing trend of NPA atomic charges for the H-acceptor, H-transferred and H-donor in R1-1 is generally similar to that of the case in R2-1 (see Fig. S5), indicating that the nature of $CH_2OO + HO_2/H_2O_2$ addition mechanism is the same that the $CH_2OO + H_2O_2$ reaction also follows a hydrogen atom transfer mechanism.

The addition reactions of $4CH_2OO + H_2O_2$ proceed by the barrierless formations of pre-reactive complexes (IM2-1, 2-2, 2-3, and 2-4) in which the two moieties are held together by hydrogen bonds between one of the hydrogen atoms of reactants (H_2O_2, P2-1, P2-2 and P2-3) and the terminal oxygen atom of CH_2OO, and by van der Waals interactions between the reactants terminal oxygen atom and the CH_2OO

central carbon atom (see Fig. S2). The relative energies of RCs (IM2-1, 2-2, 2-3 and 2-4) with respect to the respective reactants are -10.6, -12.8, -14.3 and -7.9 kcal·mol^{-1}, respectively. The barriers of these four addition reactions are decreased in the order of 7.1(TS2-3) > 6.1(TS2-1) > 4.6(TS2-2) = 4.6(TS2-4) kcal·mol^{-1}. This result indicates that the last two addition reactions R2-2 and R2-4 are preferable dynamically, and the rate-determining step is R2-3 of the whole reactions. As seen from the geometrical parameters of TS2-1, 2-2, 2-3 and 2-4 shown in Fig. S2, the breaking O-H bonds are elongated by 10.5, 13.2, 12.1 and 11.6% compared to the respect complexes equilibrium structures; whereas the distances of the forming C-O bond are 2.076, 2.136, 2.129 and 2.161 Å. The result shows that these four transition states are structurally much closer to the reactant than to the products, which are in good agreement with the characters of highly exothermic. These findings are also in line with the Hammond's principle[61].

Compared to the barriers of the 4CH_2OO + HO_2 and 4CH_2OO + H_2O_2 reactions, it can be found that the first two CH_2OO addition reactions in the former case are favoured obviously, while the last two CH_2OO addition reactions in the latter case are preferable. This conclusion is not fully consistent with previous results obtained by Moortgat and co-workers[24] that the oligomer formation follows the sequential addition of CIs to RO_2 radicals.

3.2 PES of *anti*-CH_3CHOO reactions with HO_2 and H_2O_2

Methyl substitution one of hydrogen atoms of CH_2OO yields two isomers, syn- and *anti*-CH_3CHOO (the different position of the CH_3 group with respect to the O-O bond)[62]. Previous theoretical calculation has proposed that syn- is more stable than *anti*-CH_3CHOO by about 3.3 kcal·mol^{-1} due to the hydrogen bond interaction between one of hydrogen atoms of the methyl group and the terminal oxygen atom[31]. However, the existence of intramolecular hydrogen bond limits its actively reactive for the syn-CH_3CHOO chemistry. Moreover, the steric repulsion between the methyl group and the terminal oxygen in the same side is also significant. The conclusion is further supported by recent literature report that the *anti*-conformer is more reactive

compared to the syn-conformer in the atmosphere[62-63]. Therefore, in the present study, the syn-CH_3CHOO + HO_2/H_2O_2 systems are not taken into consideration. We choose the *anti*-conformer serves as the repeat unit (n=4) to investigate the oligomer formations in the reactions with HO_2 and H_2O_2. Fig. 4 shows the potential energy surface of addition reactions of *anti*-CH_3CHOO with HO_2 and H_2O_2 at the MP2//B3LYP/6-311+G(2df,2p) level of theory.

As shown in Fig. 4, we see that the sequential additions of *anti*-CH_3CHOO to HO_2 and H_2O_2 are also strongly exothermic (> 210 kcal·mol^{-1}). The reactions proceed by the barrierless formations of pre-reactive complexes in the entrance channels followed by the submerged barriers. The results show that the consecutive reactions in the atmosphere are feasible both thermochemically and dynamically. Although the reaction paths in the formations of oligomers P3-5 and P4-4 (HOO-$(CH_3CHOO)_4$-H) are different, the chemical constitutions are completely the same. The formation mechanisms of oligomers P3-5 and P4-4 by the 4*anti*-CH_3CHOO + HO_2/H_2O_2 reactions are similar with those obtained from the $4CH_2OO$ + HO_2/H_2O_2 systems (see Scheme 1). In order to avoid redundancy, we do not repeat them here in detail. From Fig. 4(a), one can see that the pre-reactive complexes IM3-1, 3-2, 3-3, and 3-4 are formed in the entrance channel, which can be considered as the reactants (HO_2, P3-1, P3-2 and P3-3) donating a hydrogen bond to the *anti*-CH_3CHOO terminal oxygen atom. Compared to the $4CH_2OO$ + HO_2 system given in Fig 2(a), the binding energies for complexes IM3-1, 3-2, 3-3, and 3-4 are increased by 2.7, 3.6, 0.3, and 3.0 kcal·mol^{-1}, respectively.

Starting from channel R3-1, the complex IM3-1 isomerizes to the product P3-1 via transition state TS3-1 with a barrier of 1.5 kcal·mol^{-1}. Then, the polymerization reactions proceed by the sequential addition of P3-1 to *anti*-CH_3CHOO leading to the formation of product P3-4. The barriers of these four addition reactions are decreased in the order of 11.0(TS3-4) > 7.7(TS3-3) > 4.5(TS3-2) > 1.5(TS3-1) kcal·mol^{-1}, signifying that the first *anti*-CH_3CHOO addition reaction is favoured dynamically. Similar conclusion is also obtained from the calculated results of Gibbs free energies (see Table 1 and Table S4). This result also confirms the above mentioned conclusion

that the first CH_2OO addition reaction is preferable in the $4CH_2OO + HO_2$ system. The P3-4 translates into the final oligomer P3-5 by direct abstraction reaction between P3-4 and HO_2 radicals on both the singlet and triplet PESs. These two channels accompany with the barriers of 4.6 and 4.9 kcal·mol^{-1}, implying that they have nearly equivalent importance in the title reaction system. Compared to the barrier of individual elementary reaction, it can be found that the rate-determining step in the oligomer P3-5 formation is the fourth *anti*-CH_3CHOO addition reaction R3-4.

As shown in Fig. 4(b), one can see that the polymerization reactions of $4CH_3CHOO$ with H_2O_2 proceed by four step consecutive additions forming the final oligomer P4-4 (HOO-$(CH_3CHOO)_4$-H). Despite extensive efforts, we are unable to locate the transition state TS4-4 using the B3LYP functional. But it is located at the BLYP level of theory and is verified by IRC calculations. The complexes IM4-1, 4-2, 4-3, and 4-4 are formed in the entrance channels, which lie -13.0, -16.7, -19.2 and -21.5 kcal·mol^{-1}, respectively, below the energies of the respective reactants. The result shows that the binding energies of pre-reactive complexes are increased with the increase in the number of atoms involved. The barriers of these four addition reactions are 4.2, 2.7, 7.6, and 7.9 kcal·mol^{-1}, respectively, indicating that the rate-limiting step is the fourth *anti*-CH_3CHOO addition reaction (R4-4). Compared to the 4*anti*-$CH_3CHOO + HO_2$ and 4*anti*-$CH_3CHOO + H_2O_2$ systems, it can found that the first *anti*-CH_3CHOO addition reaction in the former case is favoured, while the last three *anti*-CH_3CHOO addition reactions in the latter case are advantaged. It is concluded that the predominant pathway of oligomer formation is varied with the change in the number of *anti*-CH_3CHOO involved.

For the CH_2OO/*anti*-$CH_3CHOO + HO_2/H_2O_2$ reactions, the effect of ionic property on the reaction barrier and rate coefficient is further investigated by the analysis of NPA charges, which are determined by the natural bond orbital (NBO) analysis of the B3LYP-D3 functional. And the result is displayed in Fig. S7. As shown in Fig. S7, the charge of CH_2OO central carbon atom C1 is positive (0.157 e) while its terminal oxygen atom O1 is negative (-0.417 e), indicating that CH_2OO intermediate indeed is a zwitterion. The CH_2OO intermediate having a hydrogen atom substituent

by methyl group in the anti-position, the charge of C1 atom becomes more positive (0.362 e) while the O1 atom charge is more negative (-0.458 e). The result shows that the methyl substituent in the anti-position will promote the raise of carbonyl oxides zwitterion with lower energy barriers and higher reaction rate (see Table 1 and 2). This conclusion is further supported by previous literature report that the carbonyl oxides with zwitterionic character have low energy barriers and react fast[64].

3.3 Rate coefficient

To the best of our knowledge, the experimental rate coefficients for CH_2OO/*anti*-CH_3CHOO reactions with HO_2/H_2O_2 have not been reported up to now. It is because their direct experimental identification and characterization have proven extremely difficult due to their rich reactivity. At present, the quantum mechanical method has developed a very efficient tool to estimate kinetic parameters in some areas, where the experimental methods are difficult to determine under the current condition. The theoretical rate coefficients of CH_2OO reaction with HO_2 reported by Long's group[13] increase in the range of 1.8×10^{-10} (200 K) to 2.2×10^{-10} (298 K) cm^3 $molecule^{-1}$ s^{-1} with rising temperature, and they exhibit a slightly positive temperature dependence. We feel that the rate coefficients are not able to maintain a constant (~2.0×10^{-10} cm^3 $molecule^{-1}$ s^{-1}) with increasing temperature because the reaction barrier is comparatively low (1.0 kcal·mol^{-1}) and the apparent activation barrier (E_{app}) is much negative (-10.8 kcal·mol^{-1}). Besides, Vereecken et al.[6] also has proposed that the rate coefficients predicted by Long's group are much overestimated. Therefore, we recomputed the rate coefficient of CH_2OO reaction with HO_2 using transition state theory with Eckart tunneling correction, on the basis of MP2//B3LYP-D3/6-311+G(2df,2p) energies and in the temperature range from 273 to 400 K. And the calculated results are listed in Table 2.

As seen from Table 2, the bimolecular rate coefficients of CH_2OO reaction with HO_2 (R1-1) decrease in the range of 1.5×10^{-11} (273 K) to 1.4×10^{-12} (400 K) cm^3 $molecule^{-1}$ s^{-1} with increasing temperature, and they exhibit a slightly negative temperature dependence. Similar behavior is also observed in the CH_2OO + H_2O_2

(R2-1) system (third column). The reason can be attributed to the apparent activation barriers E_{app} of these two addition reactions are much negative (-12.3 and -4.6 kcal·mol^{-1}). Shallcross et al.[65] concluded the same by the reaction of CH_3O_2 with BrO, that is, the rate coefficient shows a negative T-dependency. For example, we obtain theoretical rate coefficients of 7.8×10^{-12} and 4.4×10^{-14} cm^3 molecule^{-1} s^{-1} for the $CH_2OO + HO_2$ (R1-1) and $CH_2OO + H_2O_2$ (R2-1) reactions at room temperature. The difference is mainly attributed to the different binding energies of complexes and barrier heights of transition states.

Next we will discuss how the rate coefficient changes with the substitution of the methyl group in the *anti*-position. Equivalent to the $CH_2OO + HO_2/H_2O_2$ system, the bimolecular rate coefficients of *anti*-CH_3CHOO reactions with HO_2 and H_2O_2 also exhibits a negative T-dependency. In order to avoid redundancy, we will not discuss in detail in the following sections. When compared to the room temperature rate coefficient for $CH_2OO + HO_2$ reaction, 7.8×10^{-12} cm^3 molecule^{-1} s^{-1}, mentioned in the previous paragraph, the rate coefficient (1.0×10^{-09} cm^3 molecule^{-1} s^{-1}) increase by three orders of magnitude by the substituent of methyl group in the *anti*-position. Similar conclusion is also can be obtained from the other temperatures considered in our studies. However, the difference will become small gradually with the temperatures increase (from 206 (273 K) to 396 (400 K)). The binding energies of complex IM3-1 is smaller than that of IM1-1 2.7 kcal·mol^{-1}, although the barrier (1.5 kcal·mol^{-1}) of *anti*-$CH_3CHOO + HO_2$ (R3-1) reaction is slightly higher than the value of 1.1 kcal·mol^{-1} for $CH_2OO + HO_2$ (R1-1) system. Therefore, the substitution of the methyl group in the *anti*-position of the terminal oxygen atom will promote the addition reaction, and accelerate the formation of oligomers. Similar conclusion is also obtained from the $CH_2OO + H_2O_2$ and *anti*-$CH_3CHOO + H_2O_2$ systems.

The reactivity of CIs toward hydroxylic compounds is determined by their O-H bond dissociation energies (BDE), free energy change ($\Delta G_{acidity}$) and enthalpy change ($\Delta H_{acidity}$), and the results are listed in Fig. 5 and Table S6. As shown in Table S6, one can see that the k_{CR}/k_{H2O} (CH_2OO) ratios do not correlate with the bond dissociation energies, but do correlate well with $\Delta G_{acidity}$. The k_{CR}/k_{H2O} (CH_2OO) ratios decrease

with increasing $\Delta G_{acidity}$ (Fig. 5(a)), indicating that HX (X = OO, OOH) dissociation into ions becomes more energetically feasible. The same trend is observed from the values of $\Delta H_{acidity}$, which are all ~ 6 kcal·mol^{-1} larger than $\Delta G_{acidity}$. Similar behavior is observed in the ratios of k_{CR}/k_{H2O} (CH_3CHOO) and ΔG_{acidit} (Fig. 5(b)). The correlations show that the reaction involves a relatively polar transition state, which is consistent with the literature report that CIs have a zwitterionic structure that becomes increasingly ionic as the O-O bond is elongated[66, 67].

4. Conclusions

We report comprehensive theoretical results on the competition between HO_2 and H_2O_2 reactions with CH_2OO/*anti*-CH_3CHOO in the oligomer formations, including the geometrical parameters, reaction mechanisms and kinetic properties. The main conclusions are summarized as follows:

(a) The addition reactions between 4CH_2OO/*anti*-CH_3CHOO and HO_2/H_2O_2 are strongly exothermic (> 210 kcal·mol^{-1}), and the apparent activation barriers E_{app} are much negative, signifying that these reactions are energetically feasible in the atmosphere.

(b) Compared to the barriers of the 4CH_2OO + HO_2 and 4CH_2OO + H_2O_2 reactions, it can be found that the first two CH_2OO addition reactions in the former case are favoured, while the last two CH_2OO addition reactions in the latter case are advantaged. Similar conclusion is also derived from the observation of 4*anti*-CH_3CHOO + HO_2/H_2O_2 systems.

(c) The substitution of the methyl group in the *anti*-position of the terminal oxygen atom is feasible to promote the addition reaction, and to accelerate the oligomers formation in the chemistry of the atmosphere.

Supporting Information

The rotational constants (in MHz) of CH_2OO are presented in Table S1. The relative energies (ΔE_R), enthalpies (ΔH_R), free energies (ΔG_R), activation energies ($\Delta E_a^{\#}$) and free energies ($\Delta G_a^{\#}$) of the title reactions are listed in Table S2-S5. Relative rate coefficients for CH_3CHOO and CH_2OO reactions are shown in Table S6. The

optimized geometries of all the stationary points are presented in Figs. S1-S4. For the CH_2OO + HO_2/H_2O_2 reactions, the NPA atomic charges for the H-acceptor, H-transferred and H-donor as functions of the intrinsic reaction coordinate (IRC) are shown in Fig. S5. Geometries, HOMOs and HOMO-1 for IM2-1 and TS2-1 are shown in Fig. S6. The NPA charges of different atoms in the CH_2OO and CH_3CHOO are presented in Fig. S7. Atmospheric implications are added in the Supporting Information. This material is available free of charge via the Internet at http://pubs.acs.org.

Acknowledgments

This work was supported by the National Key Research and Development Program of China (2016YFA0203000) and the National Science Foundation of China (Nos. 41401567, 41573138 and 21473108). It was also partially supported by the Key Project of International Coperation of the Chinese Academy of Sciences (GJHZ1543) and the Research Grants Council of Hong Kong (PolyU 152083/14E), and Open foundation of State Key Laboratory of Loess and Quaternary Geology (SKLLQG1627).

References

(1) Zhao, Y.; Wingen, L. M.; Perraud, V.; Greaves, J.; Finlayson-Pitts, B. J. Role of the reaction of stabilized Criegee intermediates with peroxy radicals in particle formation and growth in air. *Phys. Chem. Chem. Phys.* **2015,** *17*, 12500-12514.

(2) Jimenez, J. L.; Canagaratna, M. R.; Donahue, N. M.; Prevot, A. S. H.; Zhang, Q. Evolution of organic aerosols in the atmosphere. *Science* **2009,** *326*, 1525-1529.

(3) Huang, R. J.; Zhang, Y.; Bozzetti, C.; Ho, K. F.; Cao, J. J.; Han, Y.; Daellenbach, K. R.; Slowik, J. G.; Platt, S. M.; Canonaco, F., et al. High secondary aerosol contribution to particulate pollution during haze events in China. *Nature* **2014,** *514*, 218-222.

(4) Smith, M. C.; Chang, C. H.; Chao, W.; Lin, L. C.; Takahashi, K.; Boering, K. A.; Lin, J. J. M. Strong negative temperature dependence of the simplest Criegee intermediate CH_2OO reaction with water dimer. *J. Phys. Chem. Lett.* **2015,** *6*, 2708-2713.

(5) Nguyen, T. N.; Putikam, R.; Lin, M. C. A novel and facile decay path of Criegee intermediates by intramolecular insertion reactions via roaming transition states. *J. Chem. Phys.* **2015,** *142*, 124312-6.

(6) Vereecken, L.; Harder, H.; Novelli, A. The reaction of Criegee intermediates with NO, RO_2, and SO_2, and their fate in the atmosphere. *Phys. Chem. Chem. Phys.* **2012,** *14*, 14682-14695.

(7) Chen, L.; Wang, W. L.; Wang, W. N.; Liu, Y. L.; Liu, F. Y.; Liu, N.; Wang, B. Z. Water-catalyzed decomposition of the simplest Criegee intermediate CH_2OO. *Theor. Chem. Acc.*

2016, *135*, 131-143.

(8) Li, J.; Guo, H. Full-dimensional potential energy surface and ro-vibrational levels of dioxirane. *J. Phys. Chem. A* **2016,** *120*, 2991-2998.

(9) Kuwata, K. T.; Guinn, E. J.; Hermes, M. R.; Fernandez, J. A.; Mathison, J. M.; Huang, K. A computational re-examination of the Criegee intermediate-sulfur dioxide reaction. *J. Phys. Chem. A* **2015,** *119*, 10316-10335.

(10) Stone, D.; Blitz, M.; Daubney, L.; Howes, N. U. M.; Seakins, P. Kinetics of CH_2OO reactions with SO_2, NO_2, NO, H_2O and CH_3CHO as a function of pressure. *Phys. Chem. Chem. Phys.* **2014,** *16*, 1139-1149.

(11) Berndt, T.; Kaethner, R.; Voigtländer, J.; Stratmann, F.; Pfeifle, M.; Reichle, P.; Sipilä, M.; Kulmala, M.; Olzmann, M. Kinetics of the unimolecular reaction of CH_2OO and the bimolecular reactions with the water monomer, acetaldehyde and acetone under atmospheric conditions. *Phys. Chem. Chem. Phys.* **2015,** *17*, 19862-19873.

(12) Berndt, T.; Voigtländer, J.; Stratmann, F.; Junninen, H.; Mauldin III, R. L.; Sipilä, M.; Kulmala, M.; Herrmann, H. Competing atmospheric reactions of CH_2OO with SO_2 and water vapour. *Phys. Chem. Chem. Phys.* **2014,** *16*, 19130-19136.

(13) Long, B.; Tan, X. F.; Long, Z. W.; Wang, Y. B.; Ren, D. S.; Zhang, W. J. Theoretical studies on reactions of the stabilized H_2COO with HO_2 and the $HO_2...H_2O$ complex. *J. Phys. Chem. A* **2011,** *115*, 6559-6567.

(14) Foreman, E. S.; Kapnas, K. M.; Murray, C. Reactions between Criegee intermediates and the inorganic acids HCl and HNO: kinetics and atmospheric implications. *Angew.Chem. Int.Ed.* **2016,** *55,* 10419-10422.

(15) Kidwell, N. M.; Li, H.; Wang, X.; Bowman, J. M.; Lester M. I. Unimolecular dissociation dynamics of vibrationally activated CH_3CHOO Criegee intermediates to OH radical products. *Nat. Chem.* **2016,** *8,* 509-514.

(16) Zhang, X.; McVay, R. C.; Huang, D. D.; Dalleska, N. F.; Aumont, B.; Flagan, R. C.; Seinfeld, J. H. Formation and evolution of molecular products in α-pinene secondary organic aerosol. *Proc. Natl. Acad. Sci. U.S.A.* **2015,** *112,* 14168-14173.

(17) Kumar, M.; Francisco, J. S. Red-light-induced decomposition of an organic peroxy radical: a new source of the HO_2 radical. *Angew. Chem. Int. Ed.* **2015,** 54, 15711-15714.

(18) Kumar, M.; Francisco, J. S. Red-light initiated decomposition of hydroxy methylperoxy radical in the presence of organic and inorganic acids: implications for the HOx formation in the lower stratosphere. *J. Phys. Chem. A* **2016,** *120,* 2677-2683.

(19) Levy, H. Normal atmosphere: large radical and formaldehyde concentrations predicted. *Science* **1971,** *173,* 141-143.

(20) Zhu, C.; Kumar, M.; Zhong, J.; Li, L.; Francisco, J. S.; Zeng, X. C. New mechanistic pathways for Criegee-water chemistry at the air/water interface. *J. Am. Chem. Soc.* **2016,** *138,* 11164-11169.

(21) Kumar, M.; Zhong, J.; Francisco, J. S.; Zeng, X. C. Criegee intermediate-hydrogen sulfide chemistry at the air/water interface. *Chem. Sci.* **2017**, 8, 5385-5391.

(22) Zhong, J.; Kumar, M.; Zhu, C. Q.; Francisco, J. S.; Zeng, X. C. Surprising stability of larger Criegee intermediates on aqueous interfaces. *Angew. Chem. Int. Ed.* **2017,** *56,* 7740-7744.

(23) Enami, S.; Colussi, A. J. Efficient scavenging of Criegee intermediates on water by surface-active cis-pinonic acid. *Phys. Chem. Chem. Phys.* **2017,** *19,* 17044-17051.

(24) Sadezky, A.; Winterhalter, R.; Kanawati, B.; Römpp, A.; Spengler, B. et al. Oligomer formation during gas-phase ozonolysis of small alkenes and enol ethers: new evidence for the central role of the Criegee intermediate as oligomer chain unit. *Atmos. Chem. Phys.* **2008,** *8*, 2667-2699.

(25) Sakamoto, Y.; Inomata, S.; Hirokawa, J. Oligomerization reaction of the Criegee intermediate leads to secondary organic aerosol formation in ethylene ozonolysis. *J. Phys. Chem. A* **2013,** *117*, 12912-12921.

(26) Wolff, S.; Boddenberg, A.; Thamm, J.; Turner, W. V.; GÄb, S. Gas-phase ozonolysis of ethene in the presence of carbonyl-oxide scavengers. *Atmos. Environ.* **1997,** *31,* 2965-2969.

(27) Anglada, J. M.; Olivella, S.; Solé, A. The reaction of formaldehyde carbonyl oxide with the methyl peroxy radical and its relevance in the chemistry of the atmosphere. *Phys. Chem. Chem. Phys.* **2013,** *15*, 18921-18933.

(28) Frisch, M. J.; Trucks, G. W.; Schlegel, H. B.; Scuseria, G. E.; Robb, M. A.; Cheeseman, J. R.; Scalmani, G.; Barone, V.; Mennucci, B.; Petersson, G. A., et al. Gaussian 09, Revision D.01; Gaussian, Inc.: Wallingford, CT, 2009.

(29) Su, Y. T.; Huang, Y. H.; Witek, H. A.; Lee, Y. P. Infrared absorption spectrum of the simplest Criegee intermediate CH_2OO. *Science* **2013,** *340,* 174-176.

(30) Miliordos, E.; Xantheas, S. S. The origin of the reactivity of the Criegee intermediate: implications for atmospheric particle growth. *Angew. Chem. Int. Ed.* **2016,** *55*, 1015-1019.

(31) Long, B.; Bao, J. L.; Truhlar, D. G. Atmospheric chemistry of Criegee intermediates: unimolecular reactions and reactions with water. *J. Am. Chem. Soc.* **2016,** *138*, 14409-14422.

(32) Zheng, J.; Truhlar, D. G., Direct dynamics study of hydrogen-transfer isomerization of 1-pentyl and 1-hexyl radicals *J. Phys. Chem. A* **2009,** *113*, 11919-11925.

(33) Grimme, S.; Antony, J.; Ehrlich, S.; Krieg, H. A consistent and accurate ab initio parametrization of density functional dispersion correction (DFT-D) for the 94 elements H-Pu. *J. Chem. Phys.* **2010,** *132,* 154104-19.

(34) Su, Y. T.; Lin, H. Y.; Putikam, R.; Matsui, H.; Lin, M. C.; Lee, Y. P. Extremely rapid self-reaction of the simplest Criegee intermediate CH_2OO and its implications in atmospheric chemistry. *Nat. Chem.* **2014,** *6*, 477-483.

(35) Buras, Z. J.; Elsamra, R. M. I.; Jalan, A.; Middaugh, J. E.; Green, W. H. Direct kinetic measurements of reactions between the simplest Criegee intermediate CH_2OO and alkenes. *J. Phys. Chem. A* **2014,** *118*, 1997-2006.

(36) Fukui, K. The path of chemical reactions - the IRC approach. *Acc. Chem. Res.* **1981,** *14*, 363-368.

(37) Page, M.; Mclver, J. W. On evaluating the reaction path Hamiltonian. *J. Chem. Phys.* **1988,** *88*, 922-935.

(38) Gonzalez, C.; Schlegel, H. B. An improved algorithm for reaction path following. *J. Chem. Phys.* **1989,** *90*, 2154-2161.

(39) Gonzalez, C.; Schlegel, H. B. Reaction path following in mass-weighted internal coordinates. *J. Phys. Chem.* **1990,** *94*, 5523-5527.

(40) Contreras-García, J.; Boto, R. A.; Izquierdo-Ruiz, F.; Reva, I.; Woller, T.; Alonso, M. A benchmark for the non-covalent interaction (NCI) index or … is it really all in the geometry? *Theor. Chem. Acc.* **2016,** *135*, 242-255.

(41) Eckart, C. The penetration of a potential barrier by electrons. *Phys. Rev.* **1930,** *35*, 1303-1309.

(42) Johnston, H. S.; Heicklen, J. Tunneling corrections for unsymmetrical Eckart potential energy barriers. *J. Phys. Chem.* **1962,** *66*, 532-533.

(43) Garrett, B. C.; Truhlar, D. G. Semiclassical tunneling calculations. *J. Phys. Chem.* **1979,** *83*, 2921-2926.

(44) Duncan, W. T.; Bell, R. L.; Truong, T. N. TheRate: program for *ab initio* direct dynamics calculations of thermal and vibrational-state-selected rate constants. *J. Comput. Chem.* **1998,** *19*, 1039-1052.

(45) Zhang, T. L.; Wang, W. L.; Zhang, P.; Lu, J.; Zhang, Y. Water-catalyzed gas-phase hydrogen abstraction reactions of CH_3O_2 and HO_2 with HO_2: a computational investigation. *Phys. Chem. Chem. Phys.* **2011,** *13*, 20794-20805.

(46) Zhang, P.; Wang, W. L.; Zhang, T. L.; Chen, L.; Du, Y. M.; Li, C. Y.; Lü, J. Theoretical study on the mechanism and kinetics for the self-reaction of $C_2H_5O_2$ radicals. *J. Phys. Chem. A* **2012,** *116*, 4610-4620.

(47) Ryzhkov, A. B.; Ariya, P. A., The importance of water clusters $(H_2O)_n$ (n = 2,..., 4) in the reaction of Criegee intermediate with water in the atmosphere. *Chem. Phys. Lett.* **2006,** *419*, 479-485.

(48) Chen, L.; Wang. W. L., Zhou, L. T.; Wang, W. N.; Liu, F. Y.; Li, C. Y.; Lü, J. Role of water clusters in the reaction of the simplest Criegee intermediate CH_2OO with water vapour. *Theor. Chem. Acc.* **2016,** *135*, 252-263.

(49) Huber, K. P.; Herzberg, G. Molecular spectra and molecular structure. IV. constants of diatomic molecules; Van Nostrand Reinhold Co.: New York, 1979.

(50) Li, J.; Carter, S.; Bowman, J. M.; Dawes, R.; Xie, D.; Guo, H. High-level, first-principles, full-dimensional quantum calculation of the ro-vibrational spectrum of the simplest criegee intermediate (CH_2OO). *J. Phys. Chem. Lett.* **2014,** *5*, 2364-2369.

(51) McCarthy, M. C.; Cheng, L.; Crabtree, K. N.; Martinez, O.; Nguyen, T. L.; Womack, C. C.; Stanton, J. F. The simplest Criegee intermediate (H_2C=O-O): isotopic spectroscopy, equilibrium structure, and possible formation from atmospheric lightning. *J. Phys. Chem. Lett.* **2013,** *4*, 4133-4139.

(52) Nakajima, M.; Endo, Y. Communication: Determination of the molecular structure of the simplest Criegee intermediate CH_2OO. *J. Chem. Phys.* **2013,** *139*, 101103-4.

(53) Beames, J. M.; Liu, F.; Lu, L.; Lester, M. I. UV spectroscopic characterization of an alkyl substituted Criegee intermediate CH_3CHOO. *J. Chem. Phys.* **2013,** *138*, 244307-9.

(54) NIST Chemistry Webbook, http://webbook.nist.gov/chemistry.

(55) Mansergas, A.; Anglada, J. M. Reaction mechanism between carbonyl oxide and hydroxyl radical: a theoretical study. *J. Phys. Chem. A* **2006,** *110*, 4001-4011.

(56) Müller, J. F.; Liu, Z. Nguyen, V. S.; Stavrakou, T.; Harvey, J. N.; Peeters, J. The reaction of methyl peroxy and hydroxyl radicals as a major source of atmospheric methanol. *Nat. Commun.* **2016,** *7,* 13213-11.

(57) Kumar, M.; Francisco, J. S. The role of catalysis in alkanediol decomposition: implications for general detection of alkanediols and their formation in the atmosphere. *J. Phys. Chem. A* **2015,** *119,* 9821-9833.

(58) Shenghur, A.; Weber, K. H.; Nguyen, N. D.; Sontising, W.; Tao, F. M. Theoretical study of the hydrogen abstraction of substituted phenols by nitrogen dioxide as a source of HONO. *J. Phys. Chem. A* **2014,** *118,* 11002-11014.

(59) Munoz-Rugeles, L.; Galano, A.; Raul Alvarez-Idaboy, J. Non-covalent π-π stacking interactions turn off non-adiabatic effects in proton-coupled electron transfer reactions. *Phys. Chem. Chem. Phys.* **2017,** *19,* 6969-6972.

(60) Sirjoosingh, A.; Hammes-Schiffer, S. Proton-coupled electron transfer versus hydrogen atom transfer: generation of charge-localized diabatic states. *J. Phys. Chem. A* **2011,** 115, (11), 2367-2377.

(61) Hammond, G. S. A correlation of reaction rates. *J. Am. Chem. Soc.* **1955,** *77*, 334-338.

(62) Lin, L. C.; Chang, H. T.; Chang, C. H.; Chao, W.; Smith, M. C.; Chang, C. H.; Lin, J. J.; Takahashi, K. Competition between H_2O and $(H_2O)_2$ reactions with CH_2OO/CH_3CHOO. *Phys. Chem. Chem. Phys.* **2016,** *18*, 4557-4568.

(63) Vereecken, L.; Harder, H.; Novelli, A. The reactions of Criegee intermediates with alkenes, ozone, and carbonyl oxides. *Phys. Chem. Chem. Phys.* **2014,** *16*, 4039-4049.

(64) Anglada, J. M.; González, J.; Torrent-Sucarrat, M. Effects of the substituents on the reactivity of carbonyl oxides. A theoretical study on the reaction of substituted carbonyl oxides with water. *Phys. Chem. Chem. Phys.* **2011,** *13,* 13034-13045.

(65) Shallcross, D. E.; Leather, K. E.; Bacak, A.; Xiao, P.; Lee, E. P. F.; Ng, M.; Mok, D. K. W.; Dyke, J. M.; Hossaini, R.; Chipperfield, M. P., et al. Reaction between CH_3O_2 and BrO radicals: A new source of upper troposphere lower stratosphere hydroxyl radicals. *J. Phys. Chem. A* **2015,** *119*, 4618-4632.

(66) Tobias, H. J.; Ziemann, P. J. Kinetics of the gas-phase reactions of alcohols, aldehydes, carboxylic acids, and water with the C13 stabilized Criegee intermediate formed from ozonolysis of 1-tetradecene. *J. Phys. Chem. A* **2001,** 105, 6129-6135.

(67) Enami, S.; Colussi, A. J. Reactions of Criegee intermediates with alcohols at air-aqueous interfaces. *J. Phys. Chem. A* **2017,** *121,* 5175-5182.

(68) Chao, W.; Hsieh, J. T.; Chang, C. H.; Lin, J. J. M. Direct kinetic measurement of the reaction of the simplest Criegee intermediate with water vapor *Science* **2015**, *347,* 751-4.

(69) Buszek, R. J.; Torrent-Sucarrat, M.; Anglada, J. M.; Francisco, J. S. Effects of a single water molecule on the OH + H_2O_2 reaction. *J. Phys. Chem. A* **2012,** *116*, 5821-5829.

(70) Ouyang, B.; McLeod, M. W.; Jones, R. L.; Bloss, W. J. NO_3 radical production from the reaction between the Criegee intermediate CH_2OO and NO_2. *Phys. Chem. Chem. Phys.* **2013,** *15*, 17070-17075.

(71) Taatjes, C. A.; Welz, O.; Eskola, A. J.; Savee, J. D.; Scheer, A. M. et al. Direct measurements of conformer-dependent reactivity of the Criegee intermediate CH_3CHOO. *Science* **2013,** *340*, 177-180.

(72) Sheps, L.; Scully, A. M.; Au, K. UV absorption probing of the conformer-dependent reactivity of a Criegee intermediate CH_3CHOO. *Phys. Chem. Chem. Phys.* **2014,** *16*, 26701-26706.

Table 1 The activation energies ($\Delta E_a^{\#}$), free energies ($\Delta G_a^{\#}$), and reaction enthalpies ($\Delta_r H_m$) (kcal·mol^{-1}) calculated for the reactions of CH_2OO/*anti*-CH_3CHOO + HO_2/H_2O_2

Reactions	Pathways	$\Delta E_a^{\#}$	$\Delta G_a^{\#}$ (298 K)	$\Delta_r H_m$ (298 K)
R1($4CH_2OO + HO_2$)	R1-1	1.1	2.2	-53.2
	R1-2	2.9	3.7	-55.0
	R1-3	11.4	13.7	-55.8
	R1-4	11.2	13.1	-57.3
	^{1}R1-5	0.3	0.2	-31.2
	^{3}R1-5	1.5	1.1	-35.6
R2($4CH_2OO + H_2O_2$)	R2-1	6.1	7.2	-54.9
	R2-2	4.6	6.2	-56.2
	R2-3	7.1	7.7	-62.4
	R2-4	4.6	6.4	-49.1
R3(4*anti*-$CH_3CHOO + HO_2$)	R3-1	1.5	2.8	-52.9
	R3-2	4.5	5.9	-53.0
	R3-3	7.7	10.4	-51.8
	R3-4	11.0	15.8	-54.7
	^{1}R3-5	4.6	4.0	-28.8
	^{3}R3-5	4.9	4.4	-52.6
R4(4*anti*-$CH_3CHOO + H_2O_2$)	R4-1	4.2	5.2	-51.9
	R4-2	2.7	3.6	-56.1
	R4-3	7.6	7.2	-54.3
	R4-4	7.9	6.9	-53.8

Energies computed at MP2//B3LYP-D3/6-311+G(2df,2p) level of theory; the ZPE, enthalpies and free energies corrections correspond to calculations at B3LYP-D3/6-311+G(2df,2p) level of theory

Table 2 Rate coefficient (cm^3 $molecule^{-1}$ s^{-1}) for reactions R1-1, 2-1, 3-1 and 4-1 calculated at the MP2//BLYP/6-311+G(2df,2p) level of theory

T	k_{TS1-1}	k_{TS2-1}	k_{TS3-1}	k_{TS4-1}
273	1.5×10^{-11}	5.5×10^{-14}	3.1×10^{-09}	4.4×10^{-11}
280	1.2×10^{-11}	5.1×10^{-14}	2.2×10^{-09}	3.5×10^{-11}
298	7.8×10^{-12}	4.4×10^{-14}	1.0×10^{-09}	2.0×10^{-11}
300	7.4×10^{-12}	4.3×10^{-14}	9.6×10^{-10}	1.9×10^{-11}
320	4.8×10^{-12}	3.7×10^{-14}	4.6×10^{-10}	1.1×10^{-11}
340	3.3×10^{-12}	3.2×10^{-14}	2.4×10^{-10}	7.2×10^{-12}
360	2.4×10^{-12}	2.9×10^{-14}	1.4×10^{-10}	4.8×10^{-12}
380	1.8×10^{-12}	2.6×10^{-14}	8.5×10^{-11}	3.4×10^{-12}
400	1.4×10^{-12}	2.4×10^{-14}	5.5×10^{-11}	2.5×10^{-12}

Figure Captions:

Fig. 1 Selected geometrical parameters for the partial stationary points optimized at the B3LYP-D3/6-311+G(2df,2p) level of theory (the number with superscript *a* is at the B3LYP/aug-cc-pVTZ level[5]; *b* is at the CCSD(T)-F12/aug-cc-pVTZ level[50]; *c* is at the CCSD(T)/aug-cc-pCV5Z level with ΔT correction[51]; *d* is experimental values from Ref.[52]; *e* is at the MN15-L/MG3S level[31]; *f* is at the CCSD(T) level[53]; *g* is taken from Ref.[54]; *h* is at the QCISD/6-311+G(d,p) level[55]; *i* is at the B3LYP/6-311++G(d,p) level[13]; lengths in angstroms and angles in degrees)

Fig. 2 Potential energy surfaces for the $4CH_2OO + HO_2$ (a) and $4CH_2OO + H_2O_2$ (b) reactions predicted at the MP2//B3LYP-D3/6-311+G(2df,2p) level of theory (the number with superscript a is calculated at the MP2//B3PW91-D3/6-311+G(2df,2p) level)

Fig. 3 Geometries and SOMOs for IM1-1 and TS1-1 calculated at the restricted open-shell B3LYP-D3/6-311+G(2df,2p) level of theory

Fig. 4 Potential energy surfaces for the reactions of 4*anti*-$CH_3CHOO + HO_2$ (a) and 4*anti*-$CH_3CHOO + H_2O_2$ (b) predicted at the MP2//B3LYP-D3/6-311+G(2df,2p) level of theory (the number with superscript a is calculated at the MP2//BLYP-D3/6-311+G(2df,2p) level)

Fig. 5 Hammett plot of relative rate coefficient vs reactant acidity, $\Delta G_{acidity}$, for the reactions of CH_2OO(a)/*anti*-CH_3CHOO(b) with HO_2, H_2O_2 and H_2O (CR represents competing reactants HO_2 and H_2O_2)

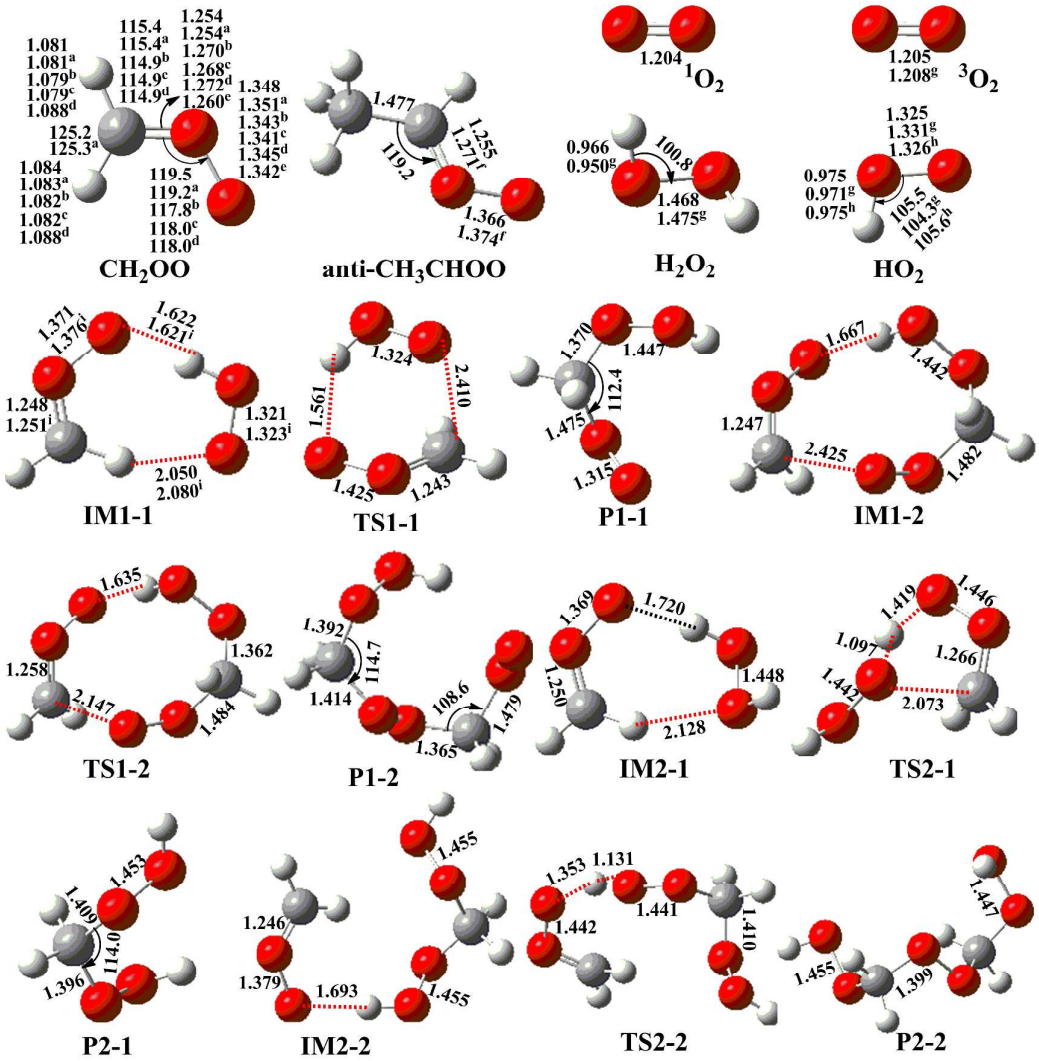
CH2OO
anti-CH3CHOO
1O2
3O2
H2O2
HO2
IM1-1
TS1-1
P1-1
IM1-2
TS1-2
P1-2
IM2-1
TS2-1
P2-1
IM2-2
TS2-2
P2-2

Fig. 1

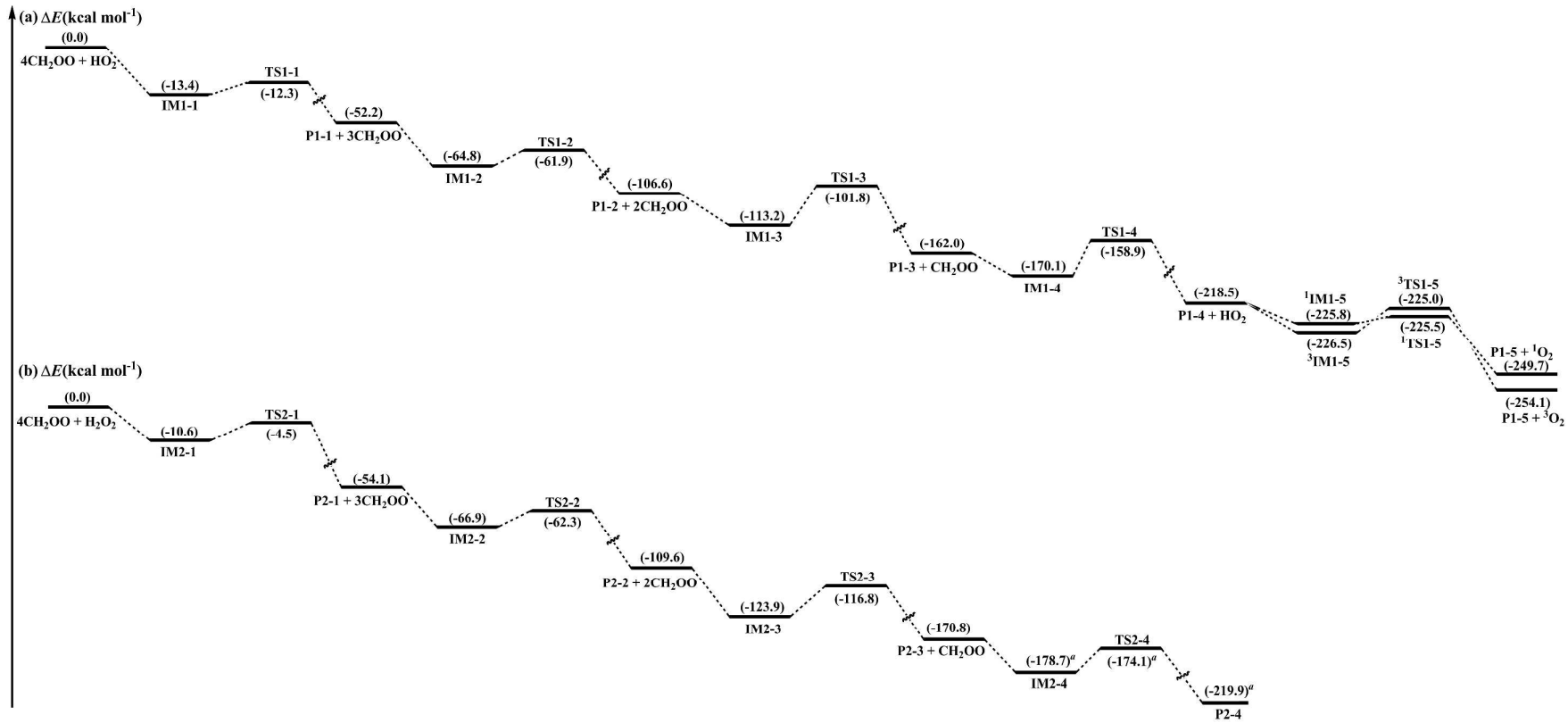
(a) ΔE(kcal mol-1)
(0.0)
4CH2OO + HO2
(-13.4)
IM1-1
TS1-1
(-12.3)
(-52.2)
P1-1 + 3CH2OO
(-64.8)
IM1-2
TS1-2
(-61.9)
(-106.6)
P1-2 + 2CH2OO
(-113.2)
IM1-3
TS1-3
(-101.8)
(-162.0)
P1-3 + CH2OO
(-170.1)
IM1-4
TS1-4
(-158.9)
(-218.5)
P1-4 + HO2
1IM1-5
(-225.8)
(-226.5)
3IM1-5
3TS1-5
(-225.0)
(-225.5)
1TS1-5
P1-5 + 1O2
(-249.7)
(-254.1)
P1-5 + 3O2
(b) ΔE(kcal mol-1)
(0.0)
4CH2OO + H2O2
(-10.6)
IM2-1
TS2-1
(-4.5)
(-54.1)
P2-1 + 3CH2OO
(-66.9)
IM2-2
TS2-2
(-62.3)
(-109.6)
P2-2 + 2CH2OO
(-123.9)
IM2-3
TS2-3
(-116.8)
(-170.8)
P2-3 + CH2OO
(-178.7)a
IM2-4
TS2-4
(-174.1)a
(-219.9)a
P2-4

Fig. 2

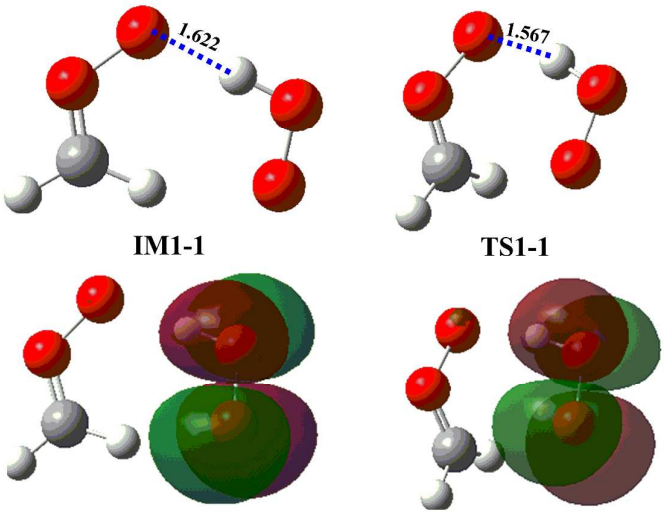

Fig. 3

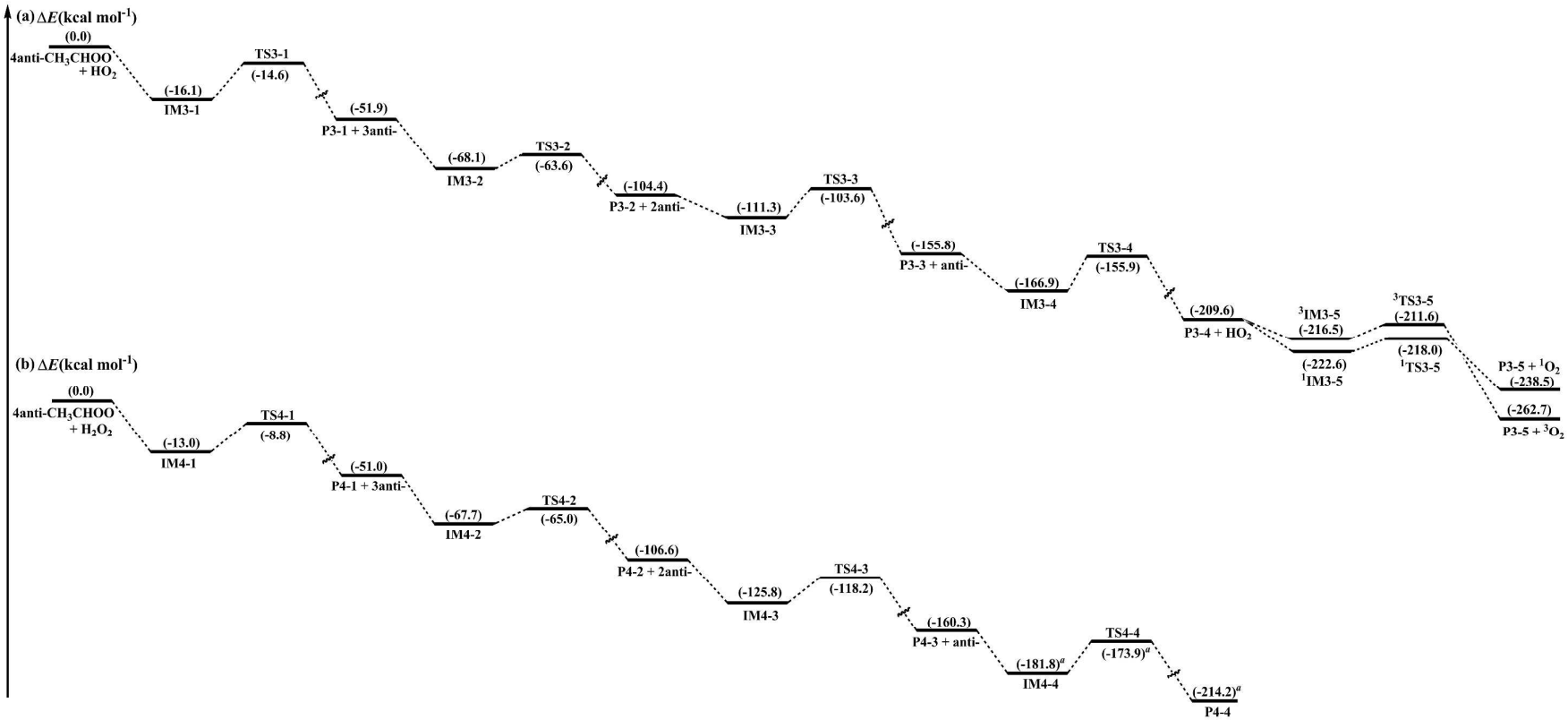
(a) ΔE(kcal mol-1)
(0.0)
4anti-CH3CHOO + HO2
(-16.1)
IM3-1
TS3-1
(-14.6)
(-51.9)
P3-1 + 3anti-
(-68.1)
IM3-2
TS3-2
(-63.6)
(-104.4)
P3-2 + 2anti-
(-111.3)
IM3-3
TS3-3
(-103.6)
(-155.8)
P3-3 + anti-
(-166.9)
IM3-4
TS3-4
(-155.9)
(-209.6)
P3-4 + HO2
3IM3-5
(-216.5)
(-222.6)
1IM3-5
3TS3-5
(-211.6)
(-218.0)
1TS3-5
P3-5 + 1O2
(-238.5)
(-262.7)
P3-5 + 3O2
(b) ΔE(kcal mol-1)
(0.0)
4anti-CH3CHOO + H2O2
(-13.0)
IM4-1
TS4-1
(-8.8)
(-51.0)
P4-1 + 3anti-
(-67.7)
IM4-2
TS4-2
(-65.0)
(-106.6)
P4-2 + 2anti-
(-125.8)
IM4-3
TS4-3
(-118.2)
(-160.3)
P4-3 + anti-
(-181.8)a
IM4-4
TS4-4
(-173.9)a
(-214.2)a
P4-4

Fig. 4

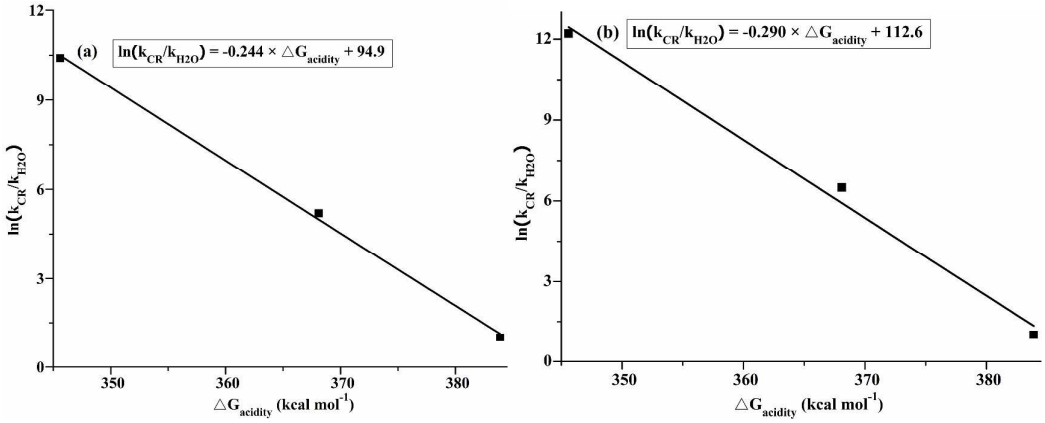
(a)
ln(k_CR/k_H2O) = -0.244 × △G_acidity + 94.9
ln(k_CR/k_H2O)
△G_acidity (kcal mol^-1)
(b)
ln(k_CR/k_H2O) = -0.290 × △G_acidity + 112.6
ln(k_CR/k_H2O)
△G_acidity (kcal mol^-1)

Fig. 5

TOC graphic

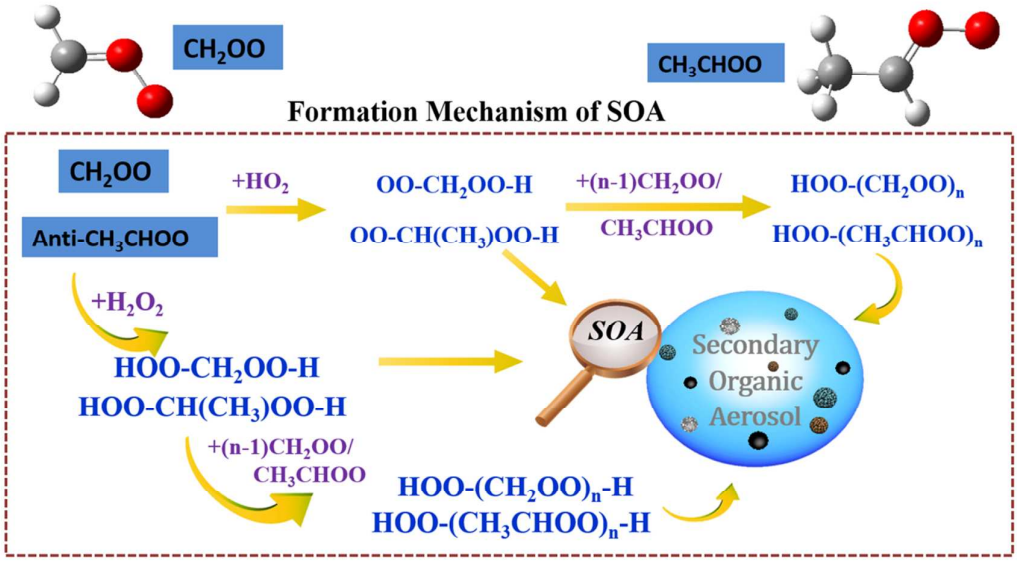
CH2OO
CH3CHOO
Formation Mechanism of SOA
CH2OO
Anti-CH3CHOO
+HO2
OO-CH2OO-H
OO-CH(CH3)OO-H
+(n-1)CH2OO/
CH3CHOO
HOO-(CH2OO)n
HOO-(CH3CHOO)n
+H2O2
HOO-CH2OO-H
HOO-CH(CH3)OO-H
SOA
Secondary
Organic
Aerosol
+(n-1)CH2OO/
CH3CHOO
HOO-(CH2OO)n-H
HOO-(CH3CHOO)n-H